MICROLANDSCAPING OF GOLD NANOPARTICLES ON GRAPHENE OXIDE FILM

WAN YIN CHI

A0067243H

A THESIS SUBMITTED FOR THE FULFILLMENT OF A DEGREE IN PHYISCS (HONOURS)

DEPARTMENT OF PHYISCS

NATIONAL UNIVERSITY OF SINGAPORE

2014

DECLARATION

I hereby declare that the thesis is my original work and it has been written by me in its entirety. I have duly acknowledged all the sources of information which have been used in the thesis

This thesis has also not been submitted for any degree in any university previously.

Wan Yin Chi

6 April 2014

ACKNOWLEDGEMENTS

It has been an exciting and fulfilling journey during the course of my final year project. Though filled with challenges and difficulties, there are several people who have both guided and accompanied me through this trying, yet meaningful journey. Here, I will like to express my deepest gratitude and sincere thanks to these wonderful people.

Firstly, I would like to thank my supervisor, Associate Professor Sow Chorng Haur, for giving me such a precious opportunity to work with him. I have learned many valuable skills and lessons from his deep knowledge and appreciation of science and research. His passion and enthusiasm is a source of motivation and inspiration for me. His never – give – up attitude encourages me to press on despite the tough challenges. His kindness and patience helps me to get back on my feet when mistakes were made. He is a person whom I deeply respect both in the field of research and in life. I would also like to thank my co – supervisor, Associate Professor Tok Eng Soon, for his guidance and advice in many aspects of my research work. The discussions I had with him cleared my doubts and helped me to gain a clearer understanding of my research work. His broad knowledge and expertise in the field of surface science imparted helped realign my focus in tackling problems that arose during my research. Without him, this work would not be possible to complete.

Another person I would like to specially thank is my mentor Teoh Hao Fatt. He has been a source of strength and encouragement throughout my research work. A fellow brother and a good friend, he was the one who helped me step by step through my entire course of research. I would like to wish him all the best for his future endeavors.

I would like to thank all the people who have helped me in one way or another during my final year project. My seniors from the nanomaterials lab, Mr. Zheng Minrui, Dr. Lu Junpeng, Dr. Lim Xiaodai Sharon, Dr. Deng Suzi, the staff from the physics department and the surface science lab, the scientists and staff from the Institute of Material Research and Engineering and from the Engineering Science Lab in the faculty of Engineering of the National University of Singapore.

I would like to thank my family members for quietly and faithfully supporting me, even at times when I failed to realize their kindness and encouragement. Their patience and understanding shown towards me during times of frustration and setbacks shall not be forgotten.

Most importantly, I would like to thank my Lord and Saviour for His grace and mercy shown towards me. I owe my entire life and being to Him. To Him be the honour, glory, and praise, forever and ever. Amen.

LIST OF FIGURES

LIST OF TABLES

ABSTRACT

Graphene, a two dimension carbon – based material, has gather much interest in research in recent years due to its unique electrical, mechanical, chemical and optical properties that can be developed into various applications with novel functionalities. A facile and versatile pathway to obtain Graphene based nanocomposites is through the reduction of Graphene Oxide (GO). Several methods of reduction that were developed include chemical, thermal, electrical, and optical process. The potential applications of GO can be expanded by incorporating metal nanoparticles (NPs) to the GO sheets. Catalytic systems, sensors, and various photovoltaic devices can be developed with the NPs – GO hybrid nanostructures.

In this thesis, we demonstrate a quick and facile method in the reduction of GO to reduced Graphene oxide (rGO) by a focused laser beam. Gold NPs were found to selectively anchor on to laser reduced areas of the GO substrate upon applying a few drops of Chloroauric acid ($HAuCl_4$). The gold – rGO nanocomposites were characterized by scanning electron microscopy and atomic force microscopy. The NPs were well – dispersed throughout the laser reduced area. The number density and size of the NPs can be tuned by varying the laser scan speed and the concentration of $HAuCl_4$ applied. The chemical composition and state of the gold NPs were studied by X – ray photoelectron spectroscopy. In addition, the gold – rGO nanocompostie was tested for Surface Enhanced Raman Spectroscopy by using Rhodamine 6G as a probe molecule. A 4 – fold enhancement was observed, and the enhancement factor was found to vary with nanoparticle size.

TABLE OF CONTENTS

CHAPTER 1 Introduction to Carbon based nanomaterials

Carbon, an element in the periodic table with an atomic number of 6, is one of the most abundant elements on Earth. It can exist as amorphous carbon, or as allotropes. Some examples of the allotropes of carbon include diamond and graphite, which has a 3 dimensional (3D) structure, Graphene, which has a 2D structure, carbon nanotubes (CNTs), which have a 1D structure, and fullerenes, which have a 0D structure. These allotropes, especially those of lower dimensions, have unique structures and properties that were previously thought not possible, spurring much research to be carried out in the past decades.

1.1 Graphene and its derivatives

Of all the allotropes of carbon, Graphene has overtaken the others to become the focus of much intense research over the past few years. The successful isolation and studies on the properties of Graphene by Andre Geim and Konstantin Novoselov back in 2004 won them the nobel prize in Physics. They reportedly measured a high carrier mobility of 10000cm^2/Vs from their Graphene sheets, which were obtained by mechanical exfoliation of highly oriented pyrolytic graphite (HOPG) [1]. Since then, Graphene has caught the interest of many researchers as it has much potential to create ground breaking progress in the field of nanoelectronics and material science.

This 2D material is made up of sp^2 hybridized carbon atoms arranged in a honeycomb lattice. Atomically thin, Graphene was found to exhibits unique electrical [2], mechanical [3], optical [4], chemical [5], and thermal properties [6]. These properties makes Graphene an ideal material for various applications, such as field effect transistors [7], flexible electronics [8], solar cells [9], energy storage devices [10], and sensors [11]. Several of these applications have been upscaled into commercial products that are now, or soon to be available to the masses [12]. Therefore, it is advantageous to develop quick and facile methods to obtain Graphene sheets that have minimal defect density, but high reproducibility.

The mechanical exfoliation of Graphene from HOPG with the help of a sticky tape was a tedious process. While the quality of Graphene produced was high with few defects, the yield of large area, single layered Graphene was low and inconsistent. New methods of fabrication of Graphene was thus developed, such as bottom – up growing by chemical vapour deposition (CVD) [13], ultrasonication in supercritical fluids to exfoliate HOPG into Graphene sheets [14], or by the reduction of Graphene oxide (GO) by thermal [15] or optical methods [16]. Recently, many researchers are starting to adopt the reduction of GO as a means to obtain derivatives of Graphene as it is a low cost, quick and facile method, having the potential in large scale applications. GO was also known to be chemically stable, and can be easily stored in a solution phase [17]. Such advantages stirred up much research on GO as they devise methods to perfect its synthesis and expand the range of applications of GO.

1.2 Graphene Oxide

GO, a derivative of Graphene, contains carboxylic, ester, and carbonyl functional groups that destroys the aromaticity of the Graphene network [18]. The carbon atoms in GO becomes sp^3 hybridized, hence losing the high electrical conductivity that Graphene posses. The electrical conductivity can be restored by the reduction of GO into reduced Graphene Oxide (rGO), albeit not to the same order of magnitude as the conductivity of Graphene. This is due to the presence of defects and vacancies that cannot be completely eliminated during reduction [19]. Nevertheless, many applications have been developed with rGO despite its shortcomings as compared to pristine Graphene, which include supercapacitors [20], sensors [21], and as a support substrate for nanoparticles [22].

Over the years, several models predicting the structure and chemical composition of GO have been proposed. One such example was the model proposed by Lerf, who used nuclear magnetic (NMR) spectroscopy to characterize a series of GO derivatives [23]. From the NMR spectra, Lerf deduced that all carbon atoms in GO are quaternary, with tertiary alcohols and epoxy (1,2 – ether) functional groups, and a mixture of alkenes. Lerf also noted the existence of strong hydrogen bonding between the alcohol and epoxide functional groups across GO sheets, giving rise to the stacked structure of GO. Subsequently, the model was revised to the well known Lerf – Klinowski model, which further proposed the presence of carboxylic acid groups at the edges of the sheets in very low quantities, along with other keto

groups. In addition, by reacting GO with several reactive species, they suggested that the double bonds in GO were either aromatic or conjugated, as isolated double bonds would be broken during the strong oxidation process to form GO [24].

The first reported synthesis of Graphene can be traced back to 1859, when Benjamin C. Brodie, a chemist from the University of Oxford, treated graphite with a mixture of fuming nitric acid and potassium chlorate [25]. The chemical formula of the product synthesized was $C_{11}H_4O_5$. Subsequently, chemist William S. Hummers and Richard E. Offeman devised a new method to synthesize GO that will take less than 2 hours, as compared to Brodie who took 3 days [26]. Their method involves treating powdered graphite flakes with a mixture of concentrated sulfuric acid and sodium nitrate, kept at a reaction temperature of 0^oC in an ice bath. Potassium permanganate was then added while the mixture was kept at a temperature below 20^oC. The Hummer's method was a faster and safer method than Brodie's, and the synthesized GO was found to have a higher degree of oxidation.

Several modifications to the Hummer's method has been developed in the recent years to improve the quality of GO synthesized. GO synthesized by the Hummer's method was found to contain large quantity of GO sediments, which are made up of multilayered graphite flakes that are oxidized at the outer layers, but pristine or mildly oxidized at the inner layers. Ang et al. reported an efficient method of intercalation and exfoliation of those graphite flakes to achieve large area GO sheets without the need for surfactants and ultrasonication [27]. Kovtyukhova et al. on the other hand suggested an additional step of oxidizing graphite prior to the Hummer's method to improve the uniformity of the degree of oxidation in the resulting GO sheets [28]. As the synthesis of GO is being perfected over time, GO is becoming a more viable option for many carbon – based applications.

1.2.1 Reduction of Graphene Oxide

One of the common reaction that GO undergoes is its reduction to rGO, with the goal to obtain composites that resemble pristine Graphene. This usually involves the removal of the functional groups present in GO, and the restoration of the π – network to the carbon backbone. Some of the typical methods used to reduce GO into rGO are chemical, thermal, electrical, and optical methods with the use of lasers. However, there is no one method, nor

combinations of methods, that can reduce GO to pristine Graphene. Each method has its own advantages, but also its shortcomings.

1.2.1.1 Chemical reduction

In the reduction of GO using chemical methods, one of the most commonly used reducing agent is hydrazine monohydrate [29]. One major reason for its popularity is its inertness to water, which is present in GO as a dispersing solvent. However, the exact reaction mechanism of hydrazine and GO is unknown. Nevertheless, by careful studies of the products of the reduction process, coupled with knowledge of the reaction mechanisms of hydrazine with other organic species, it is suggested that the reduction of GO is similar to that of the reduction of alkenes with hydrazine [30], which also leaves some functional groups intact. These functional groups, usually those with a C – N bond, cannot be easily removed by a single – step treatment. They act as n – type dopants to rGO, altering its electronic structure [31].

1.2.1.2 Thermal reduction

Another method to reduce GO is by thermal reduction, which involves heating GO to high temperatures to remove the oxygen functional groups. At 200 – 230^{o}C, desorption of the oxygen functional groups occurs [32], converting into carbon dioxide (CO_2) that are trapped between the GO layers. As the temperature is increased to 1000^{o}C, the pressure built up between layers causes the extrusion of CO_2 from within the layers, leading to the exfoliation of the GO sheets [33]. This causes structural defects and vacancies in the rGO sheets, which affects the lateral charge transport by introducing scattering sites. Nevertheless, the bulk conductivities of thermal treated rGO were found to be from 1000 – 2300 Sm^{-1}, indicating successful reduction and restoration of the π – network structure.

1.2.1.3 Electrical reduction

Recently, it has been demonstrated by Teoh et al. that GO can be reduced to rGO through an electric current [34]. They show that by applying a bias voltage at two ends of their GO substrate, the reduction process proceeds from the negative terminal to the positive terminal. Interestingly, by switching the polarity of the electrodes, reoxidation of rGO to GO occurs, and these processes of reduction and reoxidation can be repeated many times. As the experiment was carried out in ambient conditions, the strong electric field generated cause the water molecules in the air to dissociate into H^+ and OH^- ions. The H^+ ions were responsible for the reduction of GO, while the OH^- ions were responsible for the reoxidation observed. Some limitations to this methods include scalability, which is an important factor for GO to be broadly utilized.

1.2.1.4 Laser reduction

In recent years, scientists have discovered yet another method for the reduction of GO by using lasers. This method takes advantage of a combination of mechanisms to reduce GO to rGO. It is a direct, facile method that can be easily controlled. As this method of reduction is used in this work, the technique will be discussed below in greater details.

One of the processes GO undergoes when irradiated with a laser beam is photochemical reduction. According to Smimov et al., photochemical reduction is the dominant process in the reduction of GO if the wavelength of laser used is below 390nm [35]. Matsumoto et al. suggested that the small, semiconducting π – conjugated domains in GO act as photocatalysts, generating electron – hole pairs when irradiated with light with energy greater than the bandgap of the domains [36]. Together with the water molecules in the atmosphere, these electron – hole pairs are responsible for the reduction of GO to rGO. In this thesis, the wavelength of laser used for GO reduction is 532nm. Hence the reduction of GO by photochemical process is less significant in our work.

The second reduction mechanism of GO by laser irradiation is known as photothermal reduction. Similarly, photothermal reduction is the dominant process in the reduction of GO

if the wavelength of laser used is above 390nm, according to Smimov. The mechanism is similar to thermal reduction, which was mentioned above. Instead of heating the sample physically in a furnace, a laser beam is irradiated on the GO substrate. The energy from the laser creates a local hotspot, raising the temperature to as high as 500^{o}C [37].

Zhou et al. reported that for successful photothermal reduction to occur, the minimum thickness of the GO substrate is approximately 4 layers in order to absorb enough heat energy for reduction [38]. By finite element analysis, a 4 layers thick GO substrate is able to reach a temperature of >200^{o}C for desorption of the oxygen functional groups. For 6 layers and beyond, temperatures of >500^{o}C are attainable, which causes oxidative burning that leads to the sublimation and exfoliation of GO sheets. In addition, they discovered that laser reduction of GO was not effective in a nitrogen atmosphere, attributing to the lack of water molecules to facilitate the reduction.

In this thesis, a focused laser beam is irradiated on a GO substrate to selectively reduce areas of GO into rGO, allowing the creation of micropatterns and circuits. The degree of reduction can be controlled by varying the laser power and the raster scan speed of the laser beam. As mentioned earlier, there are many applications to rGO, including supercapacitors, which can be achieved by laser defining areas of rGO sandwiching a strip of GO as the dielectric on a single GO substrate [39], or as micro – sensors, which can be achieved by functionalizing the rGO surface with the sensing molecules.

1.2.2 Surface functionalization of Graphene Oxide

Surface functionalization of rGO has stirred up much interest in the field of Graphene research as it opens up many more potential applications of rGO. Due to the improved conductivity and chemical inertness of rGO, rGO becomes an excellent support substrate for various agents, ranging from bio – molecules to nanoparticles. Nanoparticles anchored to rGO were found to display improved catalytic and photovoltaic characteristics due to synergy between the two materials [40]. Shi et al. functionalized rGO sheets with DNA as a fluorescent sensor for the detection of hemin [41]. Teoh et al. decorated rGO sheets with silver nanoparticles to significantly improve the photoresponse of rGO [42]. In their work,

their silver – rGO nanocomposite was fabricated by a focused laser beam technique, and was tested for enhancement in the raman signal and for photocurrent.

1.3 Gold nanoparticles

Gold, a malleable, bright yellow metal, is a chemical element with an atomic number of 79. It is a good conductor of electricity, with a conductivity of $10^{-8}\Omega m$ [43]. It is unreactive to most chemicals, except for aqua regia, which is used to produce Chloroauric acid. Most applications of gold involve scaling it down to the nanoscale in the form of thin films or nanoparticles. As the dimensions decreases, quantum confinement effects sets in, causing new properties to arise that were previously not observed in bulk gold [44]. One such property is the existence of surface Plasmon resonance (SPR), which is the collective oscillation of mobile electrons at a characteristic frequency, trapped within a 0D quantum dot. The SPR band is sensitive to changes in the size and surface of the nanoparticles. Hence, many biosensing applications involve measuring the shift in the SPR band of gold nanoparticles to determine if a particular bio – agent is present as the bio – agent will bind itself to the surface of the gold nanoparticles [45].

Synthesis of gold nanoparticles can be traced back to the 5^{th} century B.C., where colloidal gold was used to make ruby glass and for staining ceramics, of which one famous example was the Lycurgus cup. Over the years, other methods of synthesis were developed, which include the use of surfactants and capping agents to both stabilize the NPs formed, and to have a greater control of the size and shape of the NPs. One of the more popular methods was the reduction of Chloroauric acid by sodium citrate in water, devised by Turkevitch in 1951 [46]. The NPs formed were capped with citrate ions, and were about 20nm in diameter. Later in the 1970s, Frens proposed to vary the ratio between sodium citrate and Chloroauric acid so as to control the size of the NPs formed [47]. Other methods include the use of sodium borohydrate as a reducing agent, and thiol or ligands as stabilizers [48].

Most of the gold NPs synthesized from the methods described above are capped with a stabilizing agent. While these stabilizing agents prevents aggregation of the NPs, they may modify the properties of the gold NPs, such as reducing their catalytic power in fuel cell

applications [49], or causing a broadening of the SPR band. Therefore, it is desirable to eliminate the use of reducing and stabilizing agents in the synthesis of the NPs.

Interestingly, the synthesis of gold NPs on rGO does not require the use of any reducing or stabilizing agents. Kong et al. reported the synthesis of gold nanoparticles on rGO that was first reduced from GO by a mixture of hydrazine and ammonia [50]. He proposed that the spontaneous formation of the gold NPs on rGO was due to galvanic displacement and redox reaction by relative potential difference. The standard electrode potential of rGO is 0.38V, while $AuCl_4^-$ has a higher value of +1.002V. Hence, it is possible that electrons from rGO are donated for the reduction of Au^{3+} ions. On the other hand, Moussa et al. proposed a 4 step mechanism that highlights the importance of H^+ ions from the water molecules in the GO solution [51]. The gold – rGO nanocomposites were synthesized by adding $HAuCl_4$ into GO solution, and irradiating the mixture with a pulsed laser of wavelength 532nm.

1.4 Motivation

Over the years, much work has been done in the incorporation of metallic NPs onto Graphene or its derivatives. The nanocomposites formed exhibited much potential for various applications, including catalytic systems in fuel cells, sensors, supercapacitors, and photovoltaic devices. However, very few work reported the anchoring of 2 or more different types of NPs on the same GO substrate. Most of their synthesis techniques are solution based, which results in the GO sheets being completely decorated with NPs. The ability to selectively anchor 2 different types of NPs on the same GO substrate opens doors to many exciting applications. By anchoring both TiO_2 and Pt NPs on the same sheet of rGO, we effectively put together a water splitting system, with both NPs acting as catalysts, and rGO as a medium to store and transfer charges [52]. Another possible combination is the anchoring of silver and gold NPs on rGO, which can be developed into multi – functional sensors that is able to detect both bacteria and viruses [53].

One possible solution to successfully anchor 2 or more NPs on the same GO sheet is to use a focused laser beam to selectively define areas of rGO where a certain type of nanoparticle will anchor to. Previous work done have shown the ability to decorate silver NPs only at laser reduced regions of GO. In this thesis, a direct and facile, 2 – step method to selectively

anchor gold NPs on rGO areas that has been defined by a focused laser beam will be presented. This is in line with our ultimate goal to fabricate silver – gold NPs on rGO system and determine its potential applications. The fabrication of our gold – rGO nanocomposite does not require the use of toxic reducing and capping agents to prevent the aggregation of the NPs. It is also a cost effective and quick method, with minimal wastage of metal salt solution and a submerging time of less than 1 minute. We will also study the behavior of our gold – rGO nanocomposite for enhancement in raman signal due to surface enhanced raman scattering.

CHAPTER 2 Experimental methods

2.1 Synthesis of Graphene Oxide

The GO solution used in our research was prepared by a modified Hummers' method [27]. It involved a 3 step procedure. Firstly, graphite powder was pre – oxidized in a heated solution of concentrated H_2SO_4, $K_2S_2O_8$, and P_2O_5 for 4.5 hours. The mixture was then cooled and filtered, the residue washed with DI water till the pH of filtrate reaches 5.5. The residue was dried overnight in vacuum. Next, the residue was oxidized in a solution of concentrated H_2SO_4 and $KMnO_4$ for 2 hours. The mixture was subsequently diluted with DI water, followed by the adding of H_2O_2 and leaving to stand for a day. Finally, the mixture was rinsed with HCl and acetone during filtration to remove the residual acid. The resulting residual GO stack was dried in air, which can be dispersed in water and stored as a solution for future use.

To prepare our GO sample for laser treatment, a GO solution of concentration 0.3g/L was drop – casted on a p – doped silicon wafer with a SiO_2 layer of 300nm in thickness. The sample was placed atop a hotplate kept at 70^oC. The Si substrate was cleaned by ultrasonication in acetone followed by in isopropyl alcohol for a period of 5 minutes each prior to the drop – cast of GO. A patch of GO layer was formed on the Si wafer after all the solvent has evaporated.

2.2 Fabrication of Gold – rGO sample by laser reduction

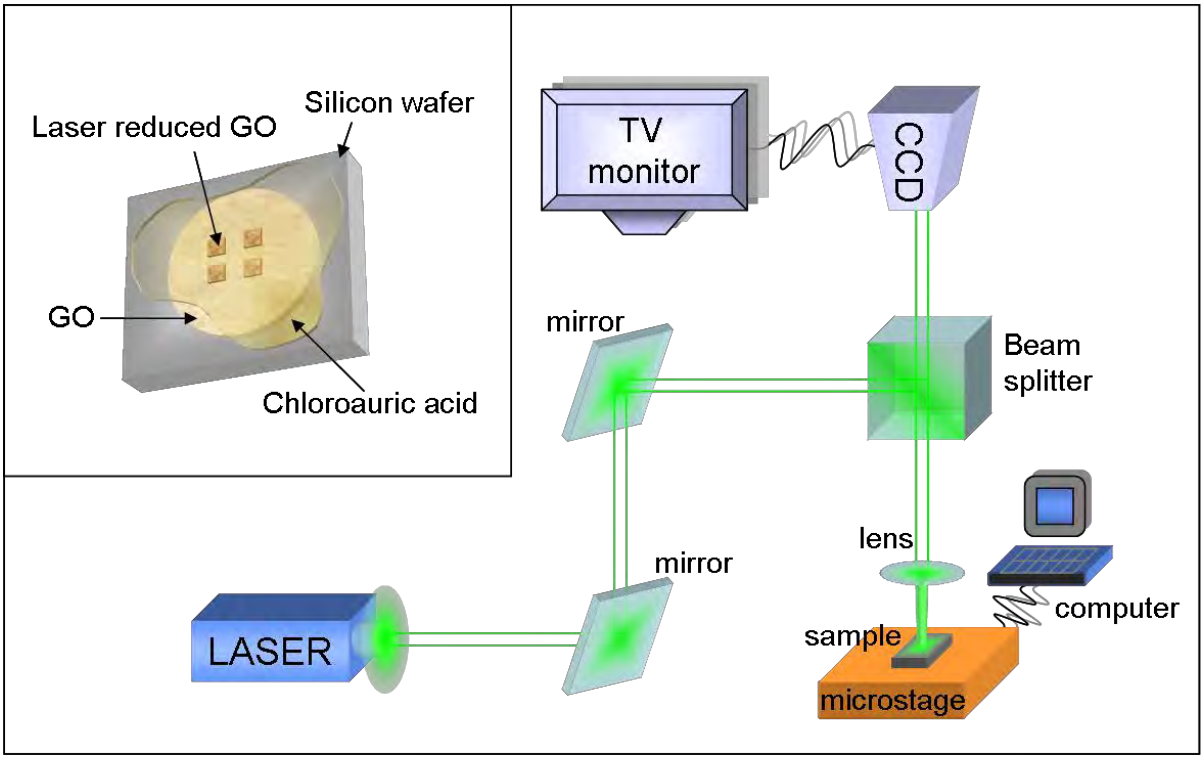

Figure 2.1: Schematic diagram of focused laser beam system. Inset shows a schematic of $HAuCl_4$ applied on to laser reduced GO supported on a silicon wafer.

Reduction of GO to rGO was achieved using a focused laser beam technique. Figure 2.1 shows the schematic of our focused laser beam set up. A laser beam of wavelength 532nm was emitted from a Suntech VD – IIIA DPSS laser. Mirrors guided the laser beam into the optical microscope, which has a beam splitter installed. The beam splitter directed the laser beam vertically downwards through a 100x microscope lens, which focused the laser beam on the GO sample. The laser spot size was approximately 1μm in diameter. The GO sample was placed on a MICOS X – Y stage, which was programmed by a computer to facilitate the drawing of patterns on the GO sample by the laser beam. A CCD camera captured the process of laser cutting and displayed the image on a TV screen for easy monitoring.

To prepare the gold – rGO nanocomposite, an area of the GO sample was first reduced by the focused laser beam. The laser power used varied from 5mW to 100mW, while the scan speed can be varied from $1\mu ms^{-1}$ to $100\mu ms^{-1}$. Once the desired pattern was formed, a few drops

of $HAuCl_4$ were applied to the laser treated regions as shown in the inset in Figure 2.1. The concentration of $HAuCl_4$ was varied from 10^{-2}M to 10^{-5}M. The sample was left to stand for 60 seconds, before being rinsed with DI water and blow dried with N_2 gas.

2.3 Characterization tools and techniques

We used several techniques and equipments to characterize our gold – rGO nanocomposites.

2.3.1 Scanning electron microscopy

The scanning electron microscope (SEM) was used to produce most of the images of our gold NPs supported on rGO. The SEM focuses a beam of high energy electrons (keV) emitted from a field emission electron gun on to the surface of our sample. By analyzing the secondary electrons emitted from the sample, an image can be formed based on the intensity of the secondary electrons collected. The model of our SEM machine is JEOL JSM – 6700F FE SEM. The beam energy was set at 5 kV, beam current at 10μA, and a chamber pressure of 96.3 μPa. Energy Dispersive X – ray (EDX) spectroscopy was also performed in – situ to determine the chemical composition of our samples.

2.3.2 Atomic force microscopy

Atomic force microscopy (AFM) utilizes a sharp cantilever probe to characterize the surface of our samples. There are two modes of imaging: contact mode and tapping mode, of which the latter is used in our experiment. By oscillating the cantilever at a certain resonance frequency, the surface topology can be mapped out by detecting changes in oscillation frequency and amplitude of the tip due to interactions with sample surface. A feedback monitor adjusts the height of the tip position to maintain a fixed tip – sample force measured. The surface roughness, step – height and depth can be obtained by analyzing the AFM images obtained. The model of our AFM machine is Digital Instruments Dimension 3000 Scanning Probe Microscope.

2.3.3 X – ray photoelectron microscopy

X – ray photoelectron spectroscopy is a surface characterization technique that utilizes X – rays to probe the chemical composition and electronic configuration of the elements present on the sample surface. X – rays incident on the sample excites the core electrons of the elements, ejecting them from the surface with a characteristic energy that depends on the binding energy of the electrons. By analyzing the kinetic energy of the photoelectrons, the identity and valence state of the elements present on the sample surface can be obtained. Measurements were carried out in a Thermal Scientific Theta Probe X – ray Spectroscopy machine at ultra – high vacuum with a monochromatic Al Kα source.

2.3.4 Raman spectroscopy

Raman spectroscopy is a non destructive technique that investigates the optical and electronic properties of a material. Based on the inelastic scattering of monochromatic light, it involves using a laser to interact with the vibrational and rotational modes of the system, resulting in a shift in the energy of the scattered photons. The model of our Raman machine is the Reinshaw inVia Raman System. A laser light of wavelength 532nm is focused on to the sample by an optical microscope with a 50x lens. The compatibility of our samples as a Surface Enhanced Raman Scattering (SERS) substrate was also investigated with a fluorescent dye, which will be further discussed in the thesis.

CHAPTER 3 Synthesis and Characterization of Gold – rGO nanocomposites

In this chapter, we demonstrate the ability to selectively anchor gold NPs on rGO areas that have been reduced by a focus laser beam. With reference to the schematic of our focused laser beam system as shown in Figure 2.1, the GO sample was placed on a microstage that is able to move in the X – Y plane, allowing the creation of the desired pattern on the GO sample as the laser raster across the surface. Subsequently, few drops of Chloroauric acid was applied on to the patterned GO so as to selectively nucleate and grow gold NPs on the laser treated rGO surface.

3.1 Ability to pattern and selectively decorate gold NPs on rGO

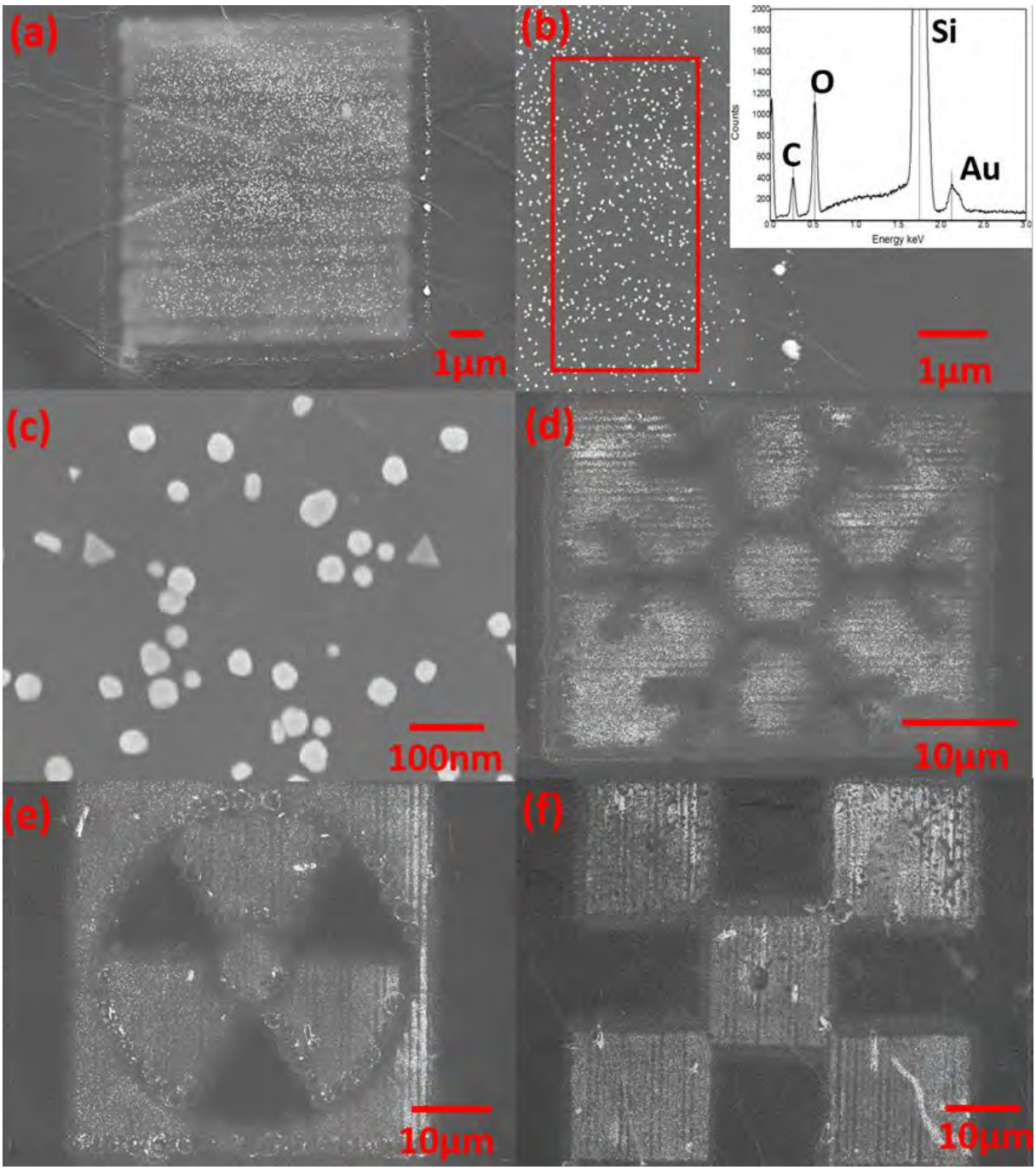

Inset: EDX spectrum indicating the presence of gold NPs

Figure 3.1: (a) – (f) SEM images of gold NPs selectively decorated on rGO.

Figure 3.1(a) shows a SEM image of a laser defined rGO square on a GO sample, with gold NPs present only within the rGO square. The NPs are well distributed throughout the rGO

square. Figure 3.1(b) shows a magnified image of the boundary of the square. EDX spectroscopy performed on an area within the square as denoted by the red box further confirmed the presence and identity of the gold NPs as shown by insert, while no gold signal was detected by EDX outside the square. High magnification shows that the NPs are approximately 50nm in diameter as shown in Figure 3.1(c), most of which have a spherical shape, while a minority taking a triangular shape. Faceted NPs forming in a triangular shape are only possible for crystalline structures, suggesting that our NPs could be single crystal gold [54]. To illustrate the strength of our focused laser beam set up in the patterning of GO, we created several designs on our GO sample and applied Chloroauric acid to decorate the laser reduced areas. Figure 3.1(d – f) show SEM images of a snowflake, a radiation hazard logo, and a checker box pattern decorated with gold NPs on a GO substrate. The dimensions of our designs are only 50μm wide, reinforcing our ability to create micro – devices and structures on GO.

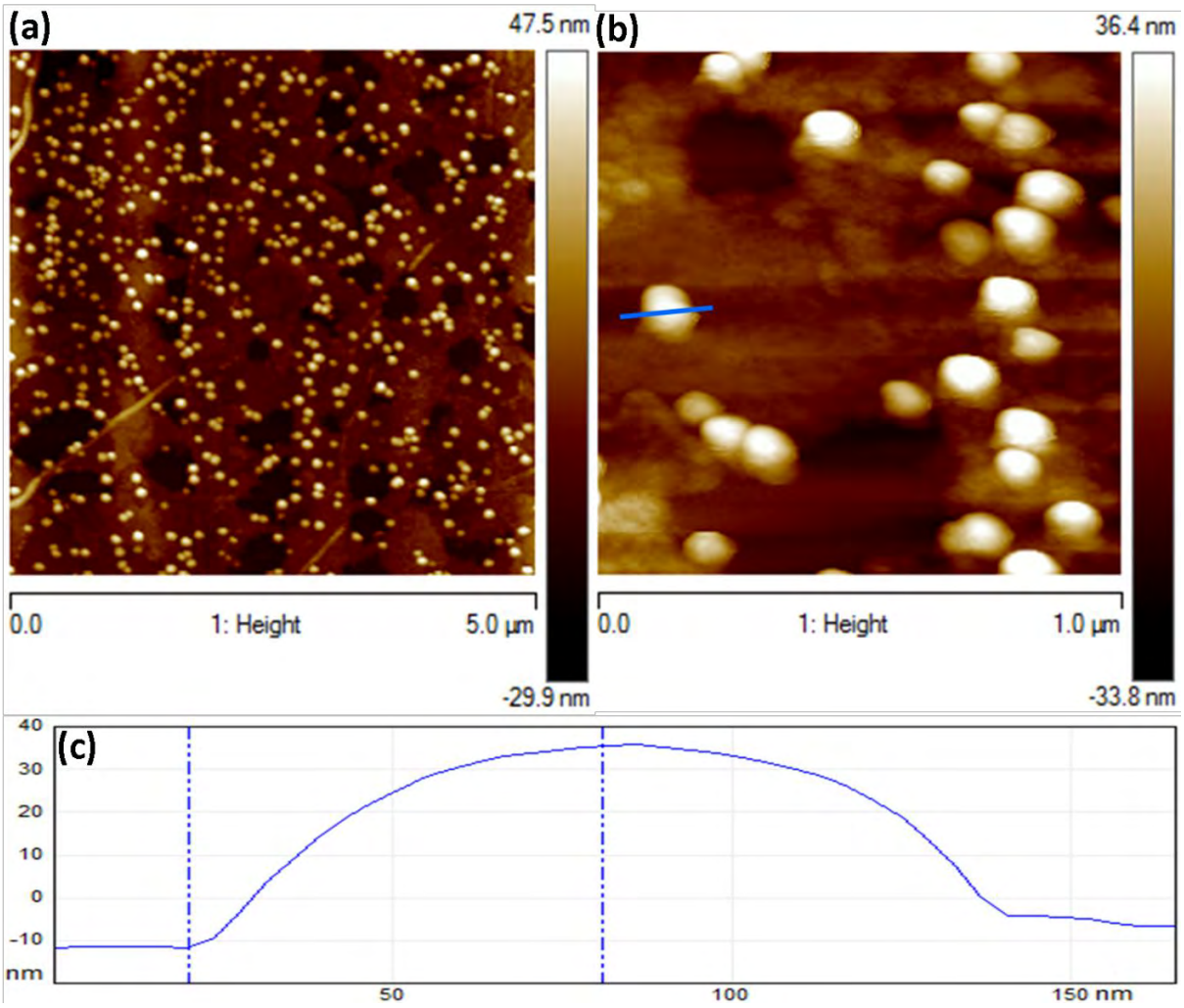

Figure 3.2: (a) – (b) AFM images of gold NPs on rGO. (c) Height profile of a single nanoparticle indicated by a blue line in (b)

AFM imaging was performed to show the topology of the surface of our Gold – rGO nanocomposites and to verify the existence of gold NPs. Figure 3.2(a) shows the gold NPs as white 'dots', well dispersed on the rGO areas. Figure 3.2(b) shows a magnified image of the gold NPs as white 'spheres', suggesting that the majority of the NPs are spherical in shape. Taking a section as shown by the blue line in Figure 3.2(b), we obtain the height profile of a single nanoparticle resting on top of the rGO as shown in Figure 3.2(c). The maximum height measured is about 45nm, which is similar to the diameter of the NPs shown in the SEM images, confirming that the gold NPs seen in the SEM images are real.

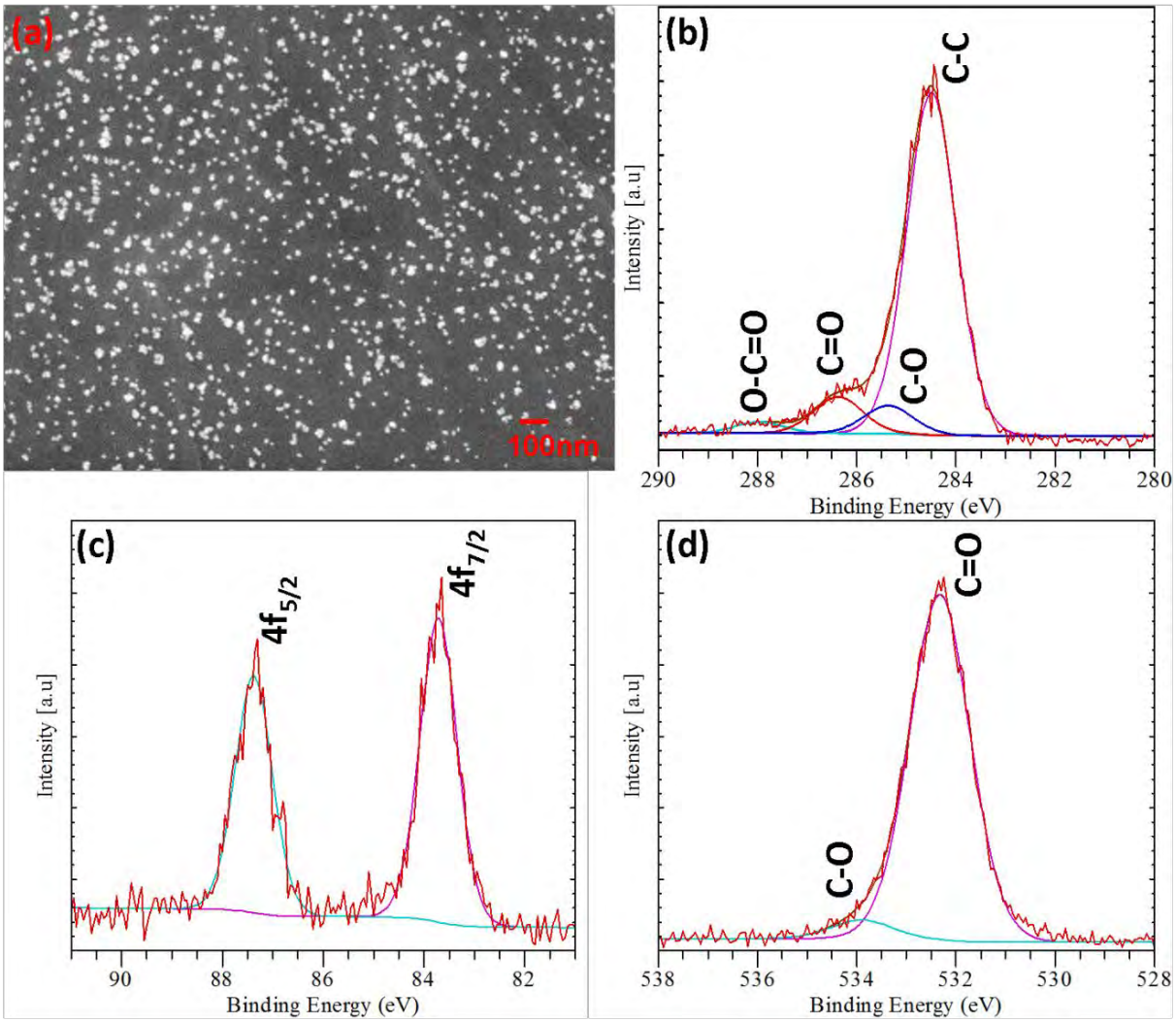

Figure 3.3: (a) SEM image of XPS sample. (b) – (d) XPS spectra of C1s, Au3f, and O1s.

XPS measurements were performed on our Au – rGO samples to determine its chemical composition. The samples were prepared by heating a 7mm by 7mm sample of GO drop – casted on a silicon wafer placed on a hotplate at 300^{o}C for 4 minutes. A few drops of $HAuCl_4$ were applied on the whole sample and left to stand for 60s, followed by washing with DI water and drying with N_2 gas. An SEM image of the sample is shown in Figure 3.3(a), with a particle size ranging from 10nm to 50nm in diameter. Figure 3.3 (b – d) shows the XPS spectra for C1s, Au4f and O1s respectively. The binding energy of C – C bond was assigned to be 284.5eV, while C – O, C = O and O – C = O have binding energies of around 285.4eV, 286.3eV and 288.0eV respectively. For O1s spectrum, the binding energies for C – O and C = O were found to be around 533.9eV and 532.3eV respectively. The error bound for the data obtained is 0.2eV. XPS spectrum for Au4f produces 2 peaks, corresponding to $Au4f_{5/2}$ and

$Au4f_{7/2}$ peaks, with binding energies to be 83.7eV and 87.3eV respectively. With reference to other literature values [55], we confirm that the chemical state of the gold NPs is Au^0.

A laser cut sample was not used for our XPS measurements due to several reasons. Firstly, a sample size of at least 3mm by 3mm is required to obtain reliable results as the beam spot size of our XPS system is of the same dimensions. However, it will take at least a week of continuous laser cutting to obtain such a sample. In addition, after applying a few drops of $HAuCl_4$, we discovered from SEM images that the number density of gold NPs formed was very low. This could be due to the loss of charges from the rGO surface to the atmospheric water vapour over time, of which more will be discussed below. Therefore, we decided to thermally reduce the GO sample as the process and mechanism is the closest to the photothermal reduction of GO.

3.2 Mechanism

To understand the mechanism of the formation of gold NPs on rGO, we first look at some mechanisms proposed by other groups. Kong et al. suggested that the formation of gold NPs on rGO is due to galvanic displacement. Zeta potential measurements of rGO reported at value of –39mV. The negatively charged rGO sheets donate electrons to facilitate the reduction of $AuCl_4^-$ ions to Au. Meanwhile, Kim et al. reported the spontaneous formation of gold NPs on Graphene sheets, most of which were located at the Graphene wrinkles [56]. Raman spectroscopy detected a shift in the G – band of GO, confirming the transfer of charges between the NPs and Graphene.

3.2.1 Charge transfer

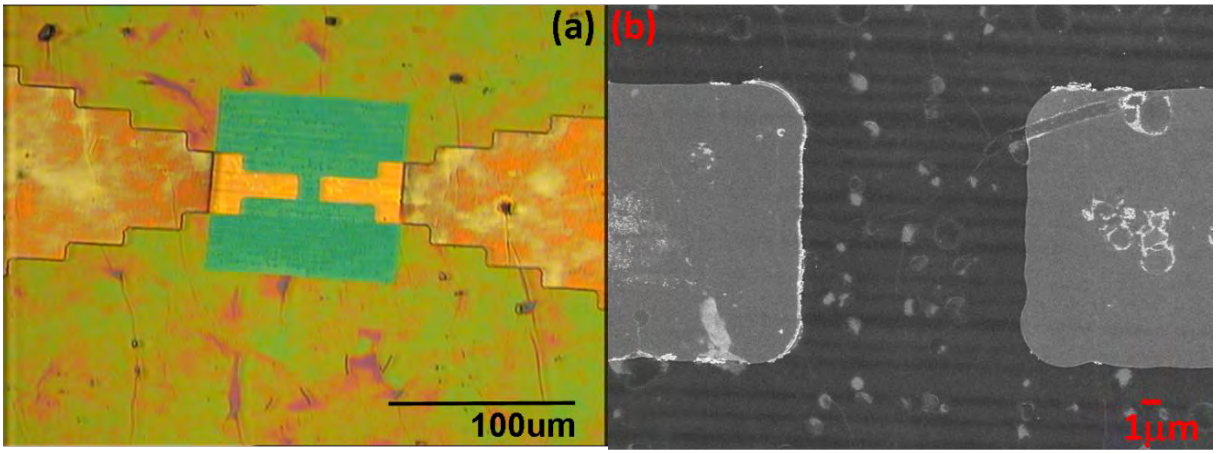

Figure 3.4: (a) Optical image of GO supported on Si wafer with gold electrodes. A 100μm and 100μm rGO square was defined by laser. (b) SEM image of rGO square.

Firstly, we verify that the formation of gold NPs on rGO is indeed due to charge transfer. We prepare a silicon substrate with gold electrodes deposited on top by photolithography methods, followed by the thermal deposition of gold on the substrate. GO drop – casted on the electrodes was reduced by laser, followed by applying $HAuCl_4$ to the laser treated regions as shown in Figure 3.4(a). Interestingly, there were no gold NPs formed on the rGO areas as seen in the SEM image shown in Figure 3.4(b). However, areas of rGO that were not directly

atop any gold electrodes shows the formation of gold NPs on the same sample. This suggests that the absence of NPs on rGO areas above the gold electrodes could be due to discharge of charges to the electrode during laser cutting. Hence, no charges are available for the formation of gold NPs. Also, ultrasonication of our Au – rGO nanocomposite in DI water for a few minutes did not show a decrease in the number density of NPs, suggesting the existence of a strong bond due to charge transfer between rGO and the gold NPs.

3.2.2 Number density vs. Laser power

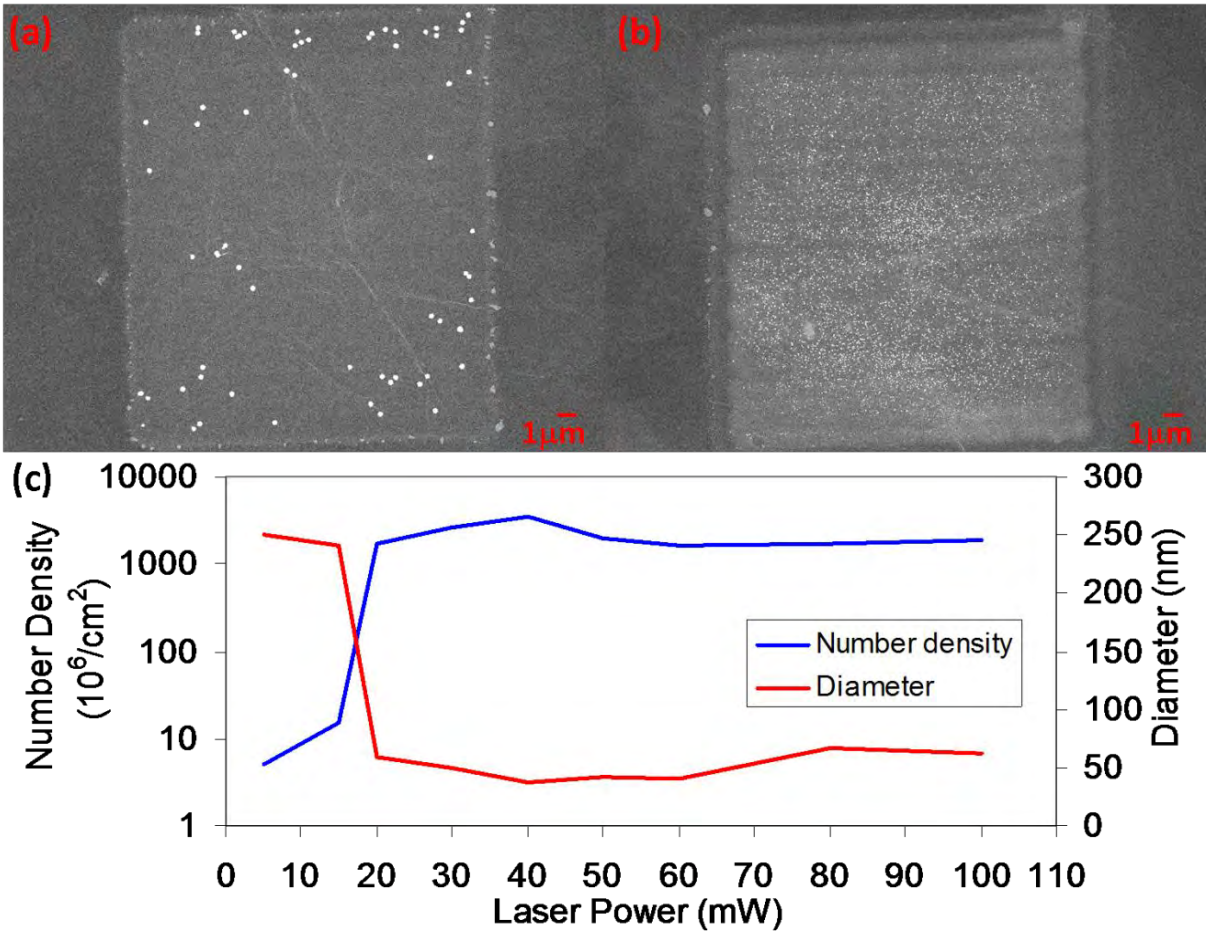

Figure 3.5: (a) – (b) SEM image of gold – rGO sample for laser powers of 15mW and 40mW respectively. (c) Plot of number density and size of NPs against laser power.

Laser defined rGO squares on a GO substrate were fabricated with different laser powers, ranging from 5mW to 100mW. After applying a few drops of $HAuCl_4$ to the squares, SEM images of the gold NPs on rGO were obtained, and the number density and size of the NPs were studied. Figure 3.5 (a – b) shows the SEM images of rGO squares reduced with laser powers 15mW and 40mW respectively. A plot of the number density and size of the NPs against laser powers used for reduction of GO is shown in Figure 3.5(c). We observed a sharp increase in the number of NPs formed for GO that was reduced with a laser power of 20mW and above, suggesting that a different mechanism may have set in at laser powers of 20mW and above. However, the size of the NPs with respect to the laser powers used followed an opposite trend compared to that for number density. This suggests that although there are

charges formed due to reduction of GO, these charges can only participate in the formation of gold NPs through active sites on the rGO. For rGO with only a few acive sites, the number of charges per active sites may be higher, hence resulting in the formation of NPs of larger diameters, but of a lower number density.

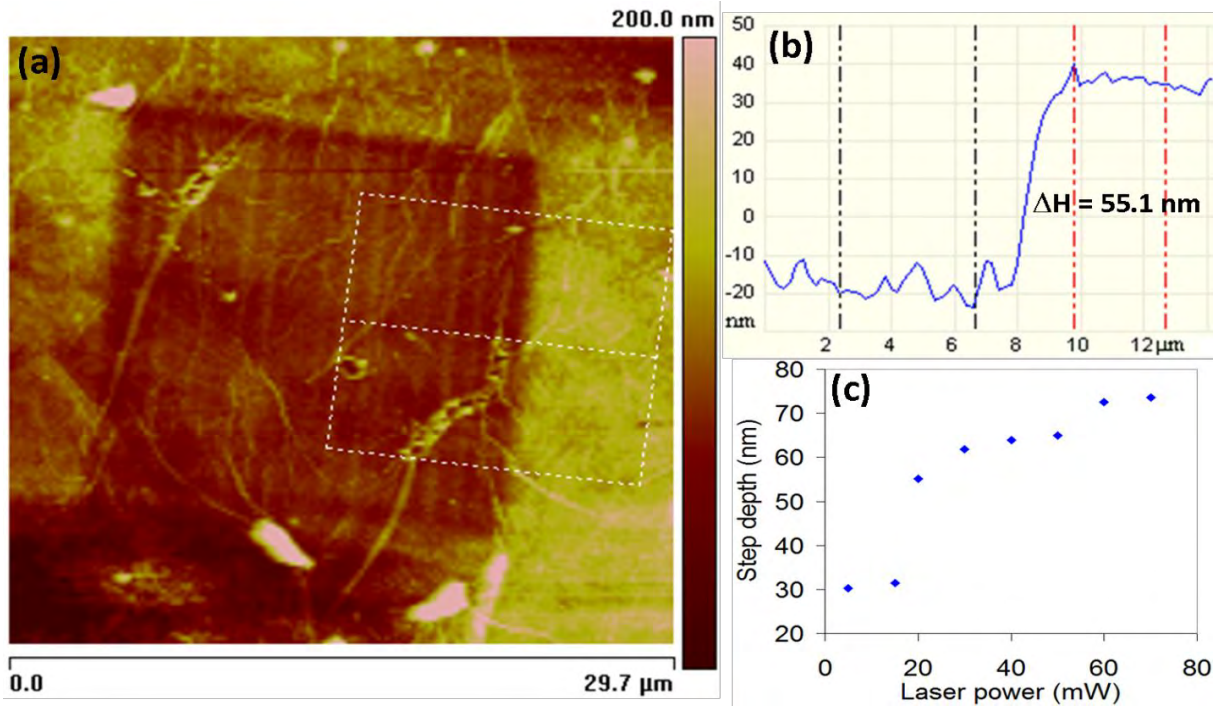

Figure 3.6: (a) AFM image of laser reduced rGO square. (b) Step depth profile of rGO square edge. (c) Plot of step depth for different laser reduction powers.

As mentioned earlier, there are 2 mechanisms that occur during photothermal reduction of GO: desorption of oxygen functional groups, which occurs at around 200^{o}C, and oxidative burning, which involves the sublimation of GO sheets at 500^{o}C. Figure 3.6(a) shows an AFM image of a rGO square cut by a laser of 20mW in power. The laser reduced areas can be identified by the change in the colour contrast. Figure 3.6(b) shows the step depth profile of an uncut region to a cut region as indicated by the white – dotted square in (a). Figure 3.6(c) shows the plot of the step depth of laser reduced GO as compared to untreated GO against different laser powers. For laser powers below 20mW, the step depth is of a relatively low value, suggesting that only the desorption of oxygen functional group has occurred. However at 20mW, we see a sharp increase in the step depth, indicating that oxidative burning of GO

sheets have set in, giving us a clue to the sharp increase in number density of gold NPs formed at 20mW.

To further understand the behaviour observed, we carried out the following experiments: 4 rGO squares reduced by laser powers of 5mW were patterned on a GO sample. However, the number of repeated scans over the same area for each square is varied from 0 to 3. After applying a few drops of $HAuCl_4$, we observe an increase in the number density of NPs for a higher number of repeated scans from SEM imaging. Optical images also show an increase in the colour contrast between the uncut regions and the laser reduced regions for each repeated scan. This indicates that further reduction of the laser reduced GO was occurring with each repeated scan. We repeat the same experiment, but with a higher laser power of 50mW. However, the number density of NPs did not increase with a higher number of repeated scans. Also, no visible change was observed from optical images for each repeated scan.

Here, we propose the following mechanism: with reference to the work done by Kim et al., which involves the spontaneous formation of gold NPs on Graphene, suggesting the existence of a bond between the carbon atoms of Graphene and gold [56], the formation of gold NPs on our laser treated rGO sample is due to the existence of dangling bonds from carbon atoms acting as sites of nucleation for gold NPs [57]. Firstly, at laser powers below 20mW, only the desorption of oxygen functional groups occurs. NPs can only be formed when an oxygen functional group is successfully removed, leaving behind the carbon atom with a dangling bond. Repeated laser scans give rise to an increase in the number density of NPs formed as each scan removes an increasing number of oxygen functional groups. Nevertheless, the desorption process is rather inefficient, resulting in only a low number density NPs formed.

However, at laser powers beyond 20mW, oxidative burning occurs, resulting in the sublimation of GO sheets. This process not only causes the successful desorption of oxygen functional groups, the high temperature also breaks the aromatic C – C bonds, resulting in a sharp increase in the number of carbon dangling bonds [58]. This translates to an abundance of nucleation sites for the formation of NPs, hence the abrupt increase in the gold NPs formed at laser power ≥20mW. Repeated scans does not show an increase in the number of NPs formed as most of the oxygen functional groups have been desorbed in the first scan due to vigorous oxidative burning. The total number of carbon dangling bonds that can be created has reach a saturation, which can be further verified by the relatively mild change in number

density of NPs formed for rGO regions that were cut at laser powers ≥20mW as shown in Figure 3.5(c).

3.2.3 Surface roughness

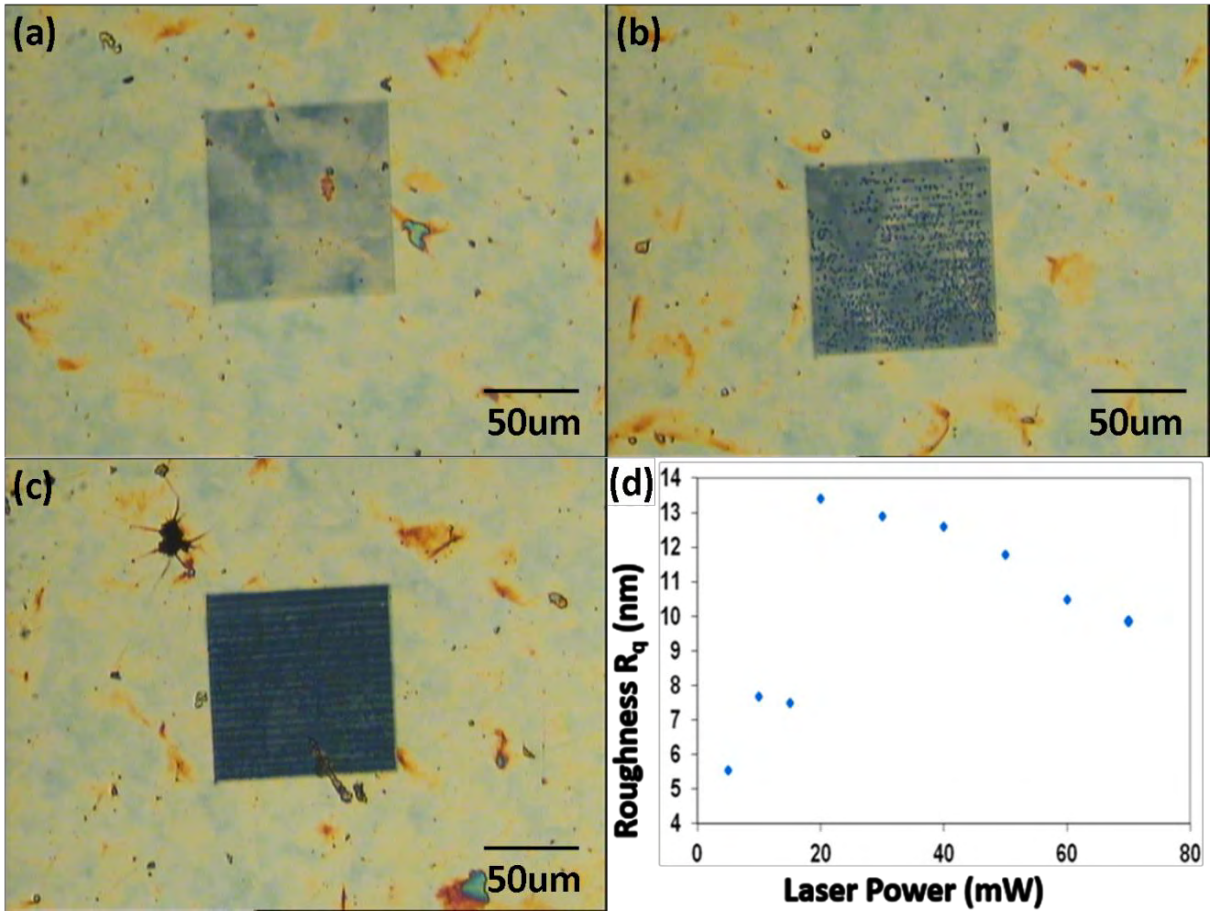

Figure 3.7: (a) – (c) Optical images of rGO squares reduced by laser of powers 15mW, 20mW and 40mW. (d) Plot of surface roughness against different laser reduction powers.

Interestingly, AFM measurements of surface roughness of rGO reduced by different laser powers show a similar trend to the number density of gold NPs formed as shown in Figure 3.7(d). A sharp increase in the surface roughness is observed for GO cut by laser with powers ≥20mW. Optical images of rGO reduced by laser powers 15mW, 20mW, and 40mW are shown in Figure 3.7(a – c). At laser powers ≥20mW, spots are seen in the rGO square, which are 'blister' like structures that formed during laser cutting. Previously in Figure 3.2(a), the blisters are visible as black patches in the AFM image. The increase in surface roughness can be attributed to the presence of these 'blisters' and the sharp increase in other physical defects caused by oxidative burning. However, as the laser power increase beyond 20mW, the surface roughness of the laser treated areas indicates a slight reduction, which is due to the annealing of GO to the substrate at higher sample temperature [59].

The similarity in trend for the number density of NPs formed and the surface roughness measured suggests that the number of physical defects on the rGO sheets facilitates the formation of gold NPs. According to thermodynamic theory, a rougher surface offers a lower Gibbs energy for the NPs to nucleate [60]. Roughening of the surface also increases the surface area available for the anchoring of the NPs [58]. The increase in the number of physical defects in the rGO network suggests an increase in the number of carbon dangling bonds available for nucleation of NPs. While there could be other factors that affect the formation of NPs on rGO that are yet to be discovered, we conclude that the number density of carbon dangling bonds and the surface roughness of rGO play significant roles.

3.3 Control and tunability

In this section, we demonstrate the ability to tune the number density and size of the gold NPs formed on rGO by varying the scan speed and the concentration of $HAuCl_4$ applied. The ability to vary the number density and size of the NPs is crucial for many applications, especially in applications that are based on the SPR and raman properties of the gold NPs.

3.3.1 Scan speed

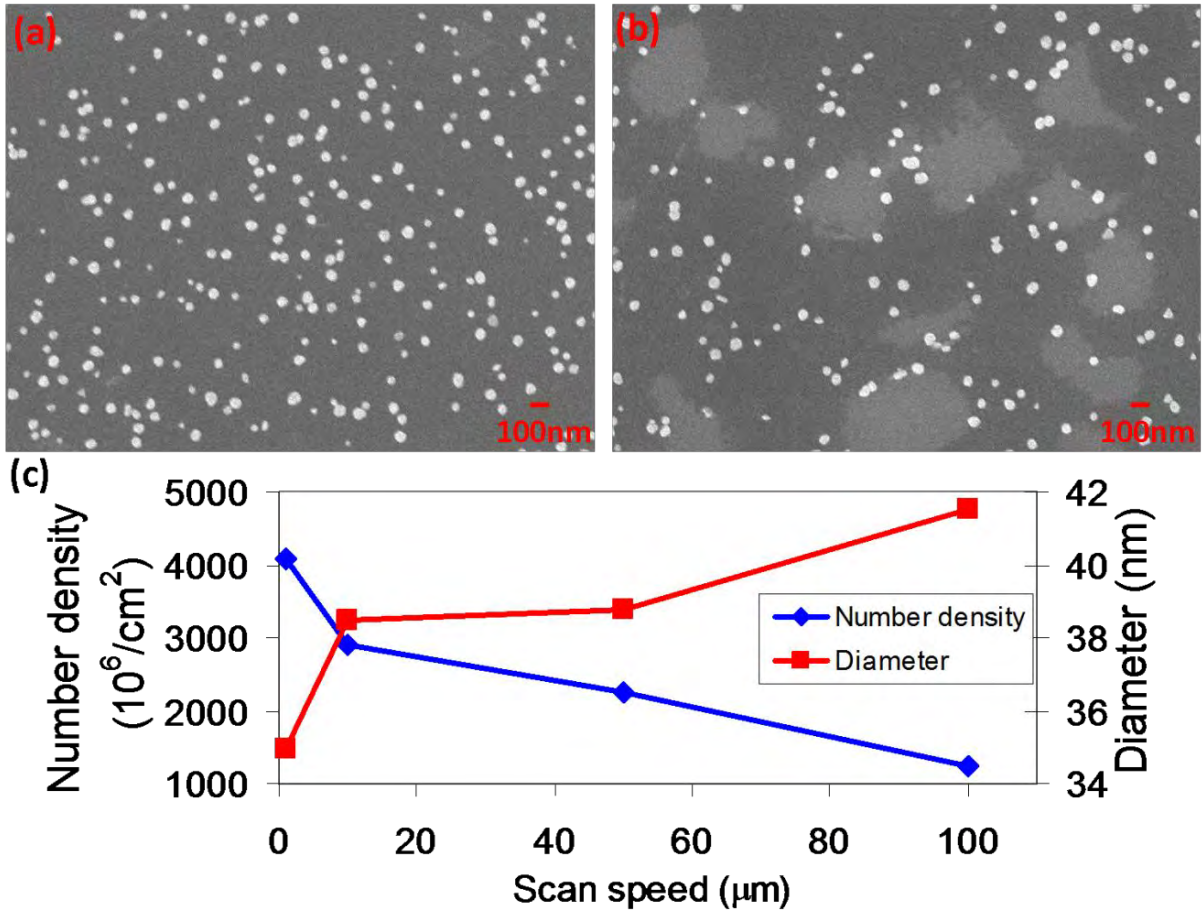

Figure 3.8: (a) – (b) SEM images of gold NPs on rGO for scan speed of 1μms^{-1} and 50μms^{-1} respectively. (c) Plot of number density and size of NPs against scan speed.

Another method to control the number density of NPs formed apart from using different laser powers as shown in section 3.2.3 is to vary the scan rate at which the laser is rastered on the GO surface. Figure 3.8 (a – b) shows the SEM images of gold NPs on rGO scanned at a

fixed laser power of 50mW, but of scan rates $1\mu ms^{-1}$ and $50\mu ms^{-1}$ respectively. As the scan rate increases, the number density of gold NPs formed decreases as shown in Figure 3.8(c). As expected, the size of the NPs formed with respect to the scan speed shows an opposite trend compared to the number density. We shall attempt to explain the above mentioned trends by performing some rough calculations.

As the scan speed is decreased, it is expected that the amount of thermal energy per unit area gained by the GO sheets also increases. To calculate the thermal energy density, we first assume that the laser energy is distributed uniformly throughout the laser spot to simplify calculations. From UV vis measurements of GO films, Krishnan and co – workers determined that the optical absorption of 1μm thick GO film in the visible range of 400nm to 800nm was about 63% [61]. For our GO samples of typical thickness ≈100nm, the absorption coefficient is then reduced to 6.3%. Using the following equation:

$$Thermal\ energy\ density = \frac{Energy}{Area} = \frac{Laser\ power}{Scan\ rate * beam\ spot\ diameter}$$

Laser power (mW)	50			
Laser spot size (μm)	1			
Scan rate (μms^{-1})	1	10	50	100
Energy (J/cm^2)	315000	31500	6300	3150

Table 3.1: Thermal energy density calculated for different scan rates.

We obtain the following thermal energy densities for different scan rates as shown in Table 3.1, for a constant laser power of 50mW and beam spot diameter of 1μm. As the thermal energy density increases, the temperature of the GO – laser hotspot increases, leading to a more effective reduction of GO and hence a larger number of NPs formed [62]. It is also worthy to mention that the deoxygenation of GO of 100nm in thickness only requires a thermal energy density of about $15Jcm^{-2}$ [61]. Comparing with our calculated values, the big differences in thermal energy densities ascertain that the oxidative burning process, which occurs during laser reduction, is indeed a vigorous process.

3.3.2 Concentration of HAuCl4

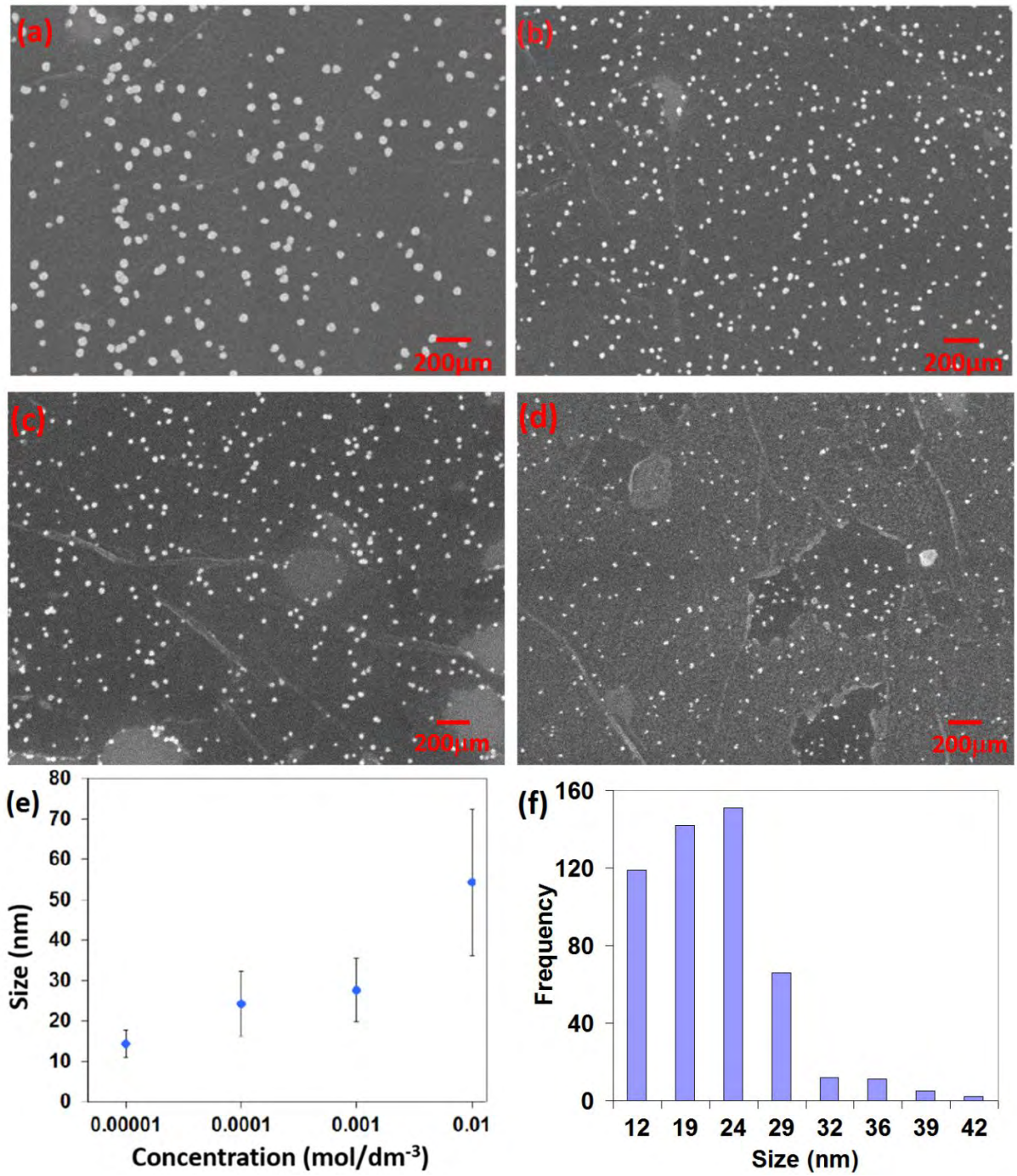

Figure 3.9: (a) – (d) SEM images of gold NPs of different sizes supported on rGO for various concentration of $HAuCl_4$ applied. (e) Plot of graph of nanoparticle size against various concentration of $HAuCl_4$. (f) Size distribution of gold NPs for a $HAuCl_4$ concentration of 0.01M

Apart from modifying the surface structure of rGO as a means to tune the number density and size of the gold NPs, varying the concentration of $HAuCl_4$ applied is also a viable option.

Figure 3.9(a – d) shows the SEM images of gold NPs formed on rGO, which was prepared by laser reduction of GO at a fixed power of 70mW, but with different concentration of 10^{-2}M, 10^{-3}M, 10^{-4}M, and 10^{-5}M of $HAuCl_4$ applied respectively. The relationship between the size of the gold NPs formed and the concentration of $HAuCl_4$ applied is plotted in Figure 3.9(e). As the concentration of $HAuCl_4$ applied increases, the average size of gold NPs formed increases, while the size distribution of the NPs widens.

2 mechanisms govern the growth of the NPs: diffusion limited or reaction limited growth. Diffusion limited growth occurs when the rate of diffusion of Au ions from bulk of solution to the nucleating NPs is the limiting factor. The NPs formed typically have a narrow size distribution. Reaction limited growth occurs when the rate of Au atoms added to the nucleating NPs is the limiting factor. The NPs formed have a wider size distribution. From Figure 3.7(d), as the size of gold NPs increase with concentration, the size distribution also widens as shown by the error bars, suggesting a shift in the mechanism of the nanoparticle growth from diffusion limited to reaction limited. Figure 3.9(f) shows the size distribution of the gold NPs for a $HAuCl_4$ concentration of 10^{-2}M. The distribution follows a asymmetric negatively skived Gaussian, which is similar to theoretical models [63]. It is also interesting to note that the growth rate and size of the NPs formed is independent of time, or perhaps reaching saturation in a very short time frame. Gold NPs formed on rGO for submerging times of 5 seconds to 15 minutes shows minor fluctuations in size and number density, reaffirming that our 2 – step synthesis is indeed a quick and easy method.

CHAPTER 4 Potential applications of the Gold – rGO nanocomposites

4.1 Surface enhanced raman scattering

Surface enhanced raman scattering, or SERS, is a surface sensitive technique that detects and characterizes the enhancement in raman signal by molecules absorbed on the surface of nanostructures, or a metallic substrate. It has various applications in the fields of biology and chemistry, such as the detection of cells [64], DNA [65], surfactants [66] and other organic compounds [67], which tend to have a weak raman signal. Although SERS was first observed in 1973 by Fleischmann and co – workers from pyridine absorbed on a roughened silver surface [68], the exact mechanism of the enhancement of raman signal is still uncertain till today. Nevertheless, 2 primary contributions to the SERS effect have been identified: the electromagnetic enhancement, and the chemical charge transfer enhancement [69].

The electromagnetic enhancement mechanism involves the excitation of localized surface plasmons of the substrate, generating an electric field that enhances the intensity of the incident light and thereby exciting the raman modes of the adsorbates. The raman signal emitted by the adsorbates are further enhanced by the same localized SPR mechanism, resulting in a strong raman signal. Typical enhancement factors are about 10^{12} times for this mechanism. The chemical charge transfer mechanism involves adsorbates that are chemisorbed to the metal surface. Excitation of charges in the absorbate – substrate system results in charge transfer transitions between the two, emitting a raman signal. Typical enhancement factors are from 10 to 100 times. These two mechanisms however are not necessarily independent of each other, and may occur simultaneously.

In this section, we investigate the efficiency of our gold – rGO nanocomposite as a SERS substrate by using Rhodamine 6G (R6G) as a probe molecule and by tuning the size of the NPs. R6G is a highly fluorescent dye that has been used by various works to evaluate the SERS properties of metallic NPs [70]. GO substrates reduced by laser at a constant laser power of 70mW were applied with $HAuCl_4$ of varying concentrations to attain gold NPs of different sizes. Subsequently, R6G of concentration of $4*10^{-3}$M was applied to each sample for a period of 20 minutes before blow drying with N_2. The Raman enhancements of the Au –

rGO substrates for different sizes of gold NPs were compared with a rGO sample with only R6G applied.

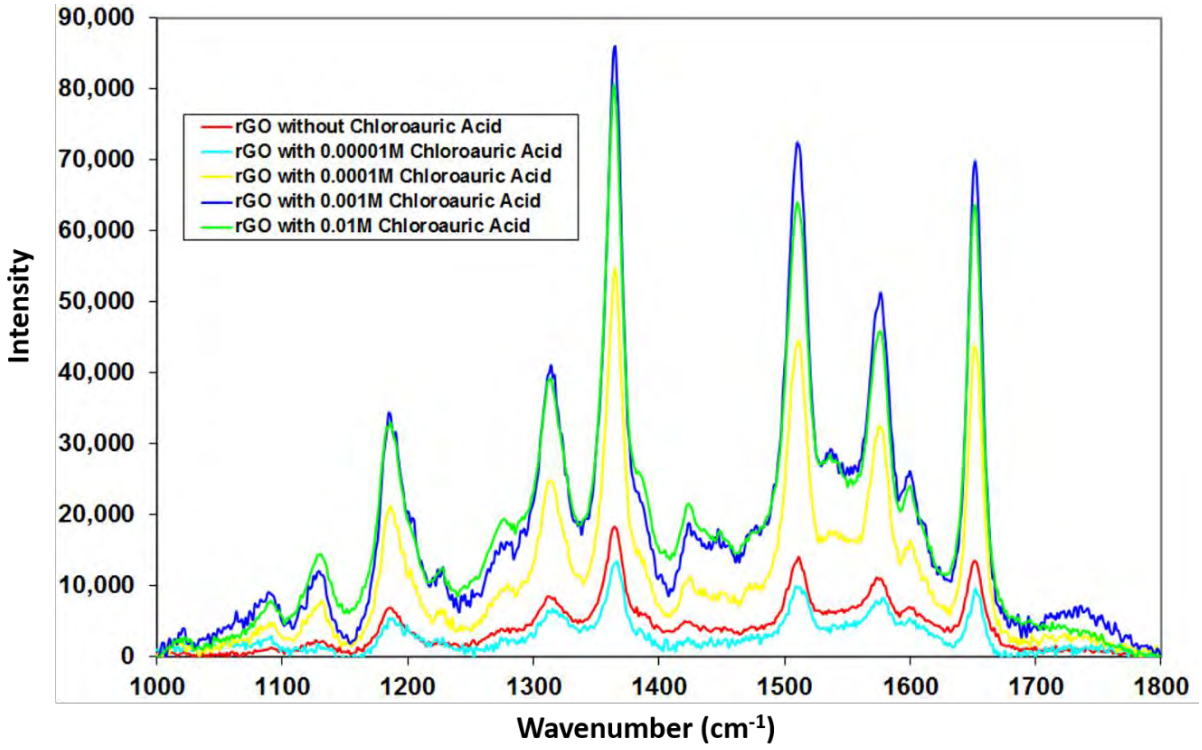

Figure 4.1: Raman spectra of gold NPs of different sizes supported on rGO. Gold NPs of differing sizes were obtained by applying different concentration of $HAuCl_4$.

Figure 4.1 shows the raman spectra of R6G supported on both rGO and Au – rGO substrates. Each raman spectra was normalized for better comparison in the extent of raman signal enhancement. As the size of the gold NPs increases, the raman intensity of R6G increases. The enhancement factors of the raman signal were about 4 times for concentrations of 0.01M and 0.001M of $HAuCl_4$ applied, and 2.5 times for 0.0001M. As the size of the gold NPs increases, the inter – nanoparticle distance decreases, resulting in a stronger electromagnetic coupling between the NPs and hence an increase in the raman signal [71]. That said, the extent of coupling between the NPs is low as the increase in raman enhancement is of a relatively small magnitude. As the size of the NPs increase further, the area of exposed rGO decreases, resulting in a decrease in the intensity of the raman signal [72]. Hence, this decrease counteracts the increase in raman signal due to coupling, as seen by the constant enhancement factor for $HAuCl_4$ concentrations of 10^{-2}M and 10^{-3}M. The magnitude of the

enhancement of raman signal suggests that charge transfer enhancement is the dominant mechanism in our Au – rGO system, reaffirming the existence of a chemical bond between rGO and the gold NPs.

Chapter 5: Conclusions and future work

5.1 Conclusions

In the first chapter, Graphene was introduced as a revolutionary material with novel properties. However, several challenges remain in the synthesis of large – area Graphene with low defect density. Reduction of Graphene Oxide was put forward as an alternative route to synthesize Graphene – based nanostructures. The potential applications of reduced Graphene oxide can be expanded by incorporating NPs on the surface of the GO sheets, which include catalytic systems and sensors. We suggested the combination of gold NPs on rGO to create a hybrid nanostructure that will give rise to interesting electronic and optical properties, and to pave the way to incorporate both gold and silver NPs on a single GO substrate based on previous works.

In this work, a quick and facile method to fabricate a gold NPs – rGO nanostructure hybrid by a focused laser beam technique was developed. We highlighted the versatility of this technique to selectively reduce areas of GO for the subsequent anchoring of gold NPs on these areas. As the diameter of the laser spot is about 1μm, the technique allows the printing of multiple micropatterns on the same GO substrate. We also proposed the existence of a chemical bond between the carbon atoms of rGO and the gold NPs. The mechanism of the formation of gold NPs involves the availability of carbon dangling bonds as nucleation sites, which is determined by the degree of reduction of GO by laser treatment. The number density and size of the gold NPs can be tuned by varying both the laser scan speed and the concentration of Chloroauric acid applied.

The gold – rGO nanocomposites were tested for Surface Enhanced Raman Scattering by using Rhodamine 6G as a probe molecule for different sizes of NPs. A 4 fold enhancement in the raman signal of R6G was recorded, suggesting the mechanism of raman signal enhancement was due to charge transfer. The enhancement of raman signal for increasing size of gold NPs depends on two conflicting factors: Increase coupling between NPs as distance between NPs decrease due to increasing size, and the decrease in exposed rGO areas due to increase shielding for larger NPs. We report an increase in the enhancement factor of the raman signal as the particle size increases, but reaching a saturation beyond a certain

particle size. Nevertheless, our gold – rGO nanocomposite is indeed a suitable SERS substrate, which can be applied in the fields of bio – sensing and chemical detection.

5.2 Future work

The work accomplished in this thesis opens the way to many exciting projects that our group may take up in the future. Firstly, a more comprehensive and in – depth research can be carried out to obtain a clearer picture in the mechanism that governs the formation of gold NPs on rGO. Kelvin probe force microscopy can be carried out to obtain a 2D map of the electronic structure and workfunction of the rGO surface for different degree of reduction. The results can be compared with the number density of NPs subsequently formed. Also, refinement can be made to the tuning of the number density and size of the NPs. Currently, the varying of both number density and size of NPs are coupled together. It will be advantageous to discover methods that can independently tune either one of the properties of the NPs formed. More precise experiments can be performed to accurately quantify the suitability of the gold – rGO nanocomposite as a SERS substrate, or for other potential applications.

Preliminary work in anchoring both silver and gold NPs on a single GO substrate has shown promising results. Firstly, gold NPs are anchored on to a rGO area that was defined by laser reduction. Subsequently, the gold – rGO sample was immersed in a solution of Silver Nitrate ($AgNO_3$). Silver NPs were deposited concurrently with the reduction of GO to rGO by laser irradiation. The anchoring of gold NPs was accomplished first as gold is less reactive than silver according to the reactivity series and hence, displacement reactions will not occur. Preliminary SEM studies have shown that both gold NPs and silver NPs are anchored on a single GO substrate in close proximity. However, further analysis and characterization of the Silver – Gold – rGO sample is required before potential applications of the hybrid system can be realized.

REFERENCES

1. Novoselov, K.S., et al., *Electric Field Effect in Atomically Thin Carbon Films.* Science, 2004. **306**(5696): p. 666 – 669.
2. Bolotin, K.I., et al., *Ultrahigh electron mobility in suspended Graphene.* Solid State Communications, 2008. **146**(9–10): p. 351 – 355.
3. Lee, C., et al., *Measurement of the Elastic Properties and Intrinsic Strength of Monolayer Graphene.* Science, 2008. **321**(5887): p. 385 – 388.
4. Gan, X., et al., *Chip – integrated ultrafast Graphene photodetector with high responsivity.* Nat Photon, 2013. **7**(11): p. 883 – 887.
5. Zhang, W., et al., *Universal Multilayer Assemblies of Graphene in Chemically Resistant Microtubes for Microextraction.* Analytical Chemistry, 2013. **85**(14): p. 6846 – 6854.
6. Balandin, A.A., et al., *Superior Thermal Conductivity of Single – Layer Graphene.* Nano Letters, 2008. **8**(3): p. 902 – 907.
7. Lemme, M.C., et al., *A Graphene Field – Effect Device.* Electron Device Letters, IEEE, 2007. **28**(4): p. 282 – 284.
8. Wang, Z. – g., et al., *Flexible Graphene – Based Electroluminescent Devices.* ACS Nano, 2011. **5**(9): p. 7149 – 7154.
9. Wang, J.T. – W., et al., *Low – Temperature Processed Electron Collection Layers of Graphene/TiO2 Nanocomposites in Thin Film Perovskite Solar Cells.* Nano Letters, 2013. **14**(2): p. 724 – 730.
10. Zhang, F., et al., *A high – performance supercapacitor – battery hybrid energy storage device based on Graphene – enhanced electrode materials with ultrahigh energy density.* Energy & Environmental Science, 2013. **6**(5): p. 1623 – 1632.
11. Schedin, F., et al., *Detection of individual gas molecules adsorbed on Graphene.* Nat Mater, 2007. **6**(9): p. 652 – 655.
12. Bae, S., et al., *Roll – to – roll production of 30 – inch Graphene films for transparent electrodes.* Nat Nanotechnol, 2010. **5**(8): p. 574 – 8.
13. Zhang, Y., L. Zhang, and C. Zhou, *Review of Chemical Vapor Deposition of Graphene and Related Applications.* Accounts of Chemical Research, 2013. **46**(10): p. 2329 – 2339.
14. Cai, M., et al., *Methods of graphite exfoliation.* Journal of Materials Chemistry, 2012. **22**(48): p. 24992 – 25002.
15. Gao, X., J. Jang, and S. Nagase, *Hydrazine and Thermal Reduction of Graphene Oxide: Reaction Mechanisms, Product Structures, and Reaction Design.* The Journal of Physical Chemistry C, 2009. **114**(2): p. 832 – 842.
16. Cote, L.J., R. Cruz – Silva, and J. Huang, *Flash Reduction and Patterning of Graphite Oxide and Its Polymer Composite.* Journal of the American Chemical Society, 2009. **131**(31): p. 11027 – 11032.
17. Kim, S., et al., *Room – temperature metastability of multilayer Graphene oxide films.* Nat Mater, 2012. **11**(6): p. 544 – 549.
18. Dreyer, D.R., et al., *The chemistry of Graphene oxide.* Chemical Society Reviews, 2010. **39**(1): p. 228 – 240.
19. Erickson, K., et al., *Determination of the Local Chemical Structure of Graphene Oxide and Reduced Graphene Oxide.* Advanced Materials, 2010. **22**(40): p. 4467 – 4472.

20. Zhao, B., et al., *Supercapacitor performances of thermally reduced Graphene oxide.* Journal of Power Sources, 2012. **198**(0): p. 423 – 427.
21. Borini, S., et al., *Ultrafast Graphene Oxide Humidity Sensors.* ACS Nano, 2013. **7**(12): p. 11166 – 11173.
22. ZHANG, H., X. HUANG, and F. BOEY, *A BRIEF REVIEW ON GRAPHENE – NANOPARTICLE COMPOSITES.* COSMOS, 2010. **06**(02): p. 159 – 166.
23. He, H., et al., *Solid – State NMR Studies of the Structure of Graphite Oxide.* The Journal of Physical Chemistry, 1996. **100**(51): p. 19954 – 19958.
24. Lerf, A., et al., *Structure of Graphite Oxide Revisited‖.* The Journal of Physical Chemistry B, 1998. **102**(23): p. 4477 – 4482.
25. Brodie, B.C., *On the Atomic Weight of Graphite.* Philosophical Transactions of the Royal Society of London, 1859. **149**: p. 249 – 259.
26. Hummers, W.S. and R.E. Offeman, *Preparation of Graphitic Oxide.* Journal of the American Chemical Society, 1958. **80**(6): p. 1339 – 1339.
27. Ang, P.K., et al., *High – Throughput Synthesis of Graphene by Intercalation−Exfoliation of Graphite Oxide and Study of Ionic Screening in Graphene Transistor.* ACS Nano, 2009. **3**(11): p. 3587 – 3594.
28. Kovtyukhova, N.I., et al., *Layer – by – Layer Assembly of Ultrathin Composite Films from Micron – Sized Graphite Oxide Sheets and Polycations.* Chemistry of Materials, 1999. **11**(3): p. 771 – 778.
29. Stankovich, S., et al., *Synthesis of Graphene – based nanosheets via chemical reduction of exfoliated graphite oxide.* Carbon, 2007. **45**(7): p. 1558 – 1565.
30. Waddell, T.G., *Advanced Organic Chemistry, 4th Edition. Part B: Reactions and Synthesis, (Sundberg, Richard J.; Carey, Francis A.).* Journal of Chemical Education, 2003. **80**(8): p. 883.
31. Kang, S.J., et al., *High – performance electronics using dense, perfectly aligned arrays of single – walled carbon nanotubes.* Nat Nano, 2007. **2**(4): p. 230 – 236.
32. Jeong, H. – K., et al., *Thermal stability of graphite oxide.* Chemical Physics Letters, 2009. **470**(4–6): p. 255 – 258.
33. Schniepp, H.C., et al., *Functionalized Single Graphene Sheets Derived from Splitting Graphite Oxide.* The Journal of Physical Chemistry B, 2006. **110**(17): p. 8535 – 8539.
34. Teoh, H.F., et al., *Electrical current mediated interconversion between Graphene oxide to reduced grapene oxide.* Applied Physics Letters, 2011. **98**(17): p. 173105.
35. Smirnov, V.A., et al., *Photoreduction of graphite oxide.* High Energy Chemistry, 2011. **45**(1): p. 57 – 61.
36. Matsumoto, Y., et al., *Photoreaction of Graphene Oxide Nanosheets in Water.* The Journal of Physical Chemistry C, 2011. **115**(39): p. 19280 – 19286.
37. Zhou, Y. and K.P. Loh, *Making Patterns on Graphene.* Advanced Materials, 2010. **22**(32): p. 3615 – 3620.
38. Zhou, Y., et al., *Microstructuring of Graphene Oxide Nanosheets Using Direct Laser Writing.* Advanced Materials, 2010. **22**(1): p. 67 – 71.
39. El – Kady, M.F., et al., *Laser Scribing of High – Performance and Flexible Graphene – Based Electrochemical Capacitors.* Science, 2012. **335**(6074): p. 1326 – 1330.
40. Yoo, E., et al., *Enhanced Electrocatalytic Activity of Pt Subnanoclusters on Graphene Nanosheet Surface.* Nano Letters, 2009. **9**(6): p. 2255 – 2259.
41. Shi, Y., et al., *A label – free DNA reduced Graphene oxide – based fluorescent sensor for highly sensitive and selective detection of hemin.* Chemical Communications, 2011. **47**(16): p. 4676 – 4678.
42. Teoh, H.F., et al., *Microlandscaping on a Graphene oxide film via localized decoration of Ag nanoparticles.* Nanoscale, 2014. **6**(6): p. 3143 – 3149.

43. Matula, R.A., *Electrical resistivity of copper, gold, palladium, and silver.* Journal of Physical and Chemical Reference Data, 1979. **8**(4): p. 1147 – 1298.
44. Ung, T., L.M. Liz – Marzán, and P. Mulvaney, *Gold nanoparticle thin films.* Colloids and Surfaces A: Physicochemical and Engineering Aspects, 2002. **202**(2–3): p. 119 – 126.
45. Wood, J.B., et al., *Fabrication of DNA Microarrays on Polydopamine – Modified Gold Thin Films for SPR Imaging Measurements.* Langmuir, 2013. **29**(34): p. 10868 – 10873.
46. Turkevich, J., P.C. Stevenson, and J. Hillier, *A study of the nucleation and growth processes in the synthesis of colloidal gold.* Discussions of the Faraday Society, 1951. **11**(0): p. 55 – 75.
47. Frens, G., *Controlled Nucleation for the Regulation of the Particle Size in Monodisperse Gold Suspensions.* Nature physical science, 1973. **241**(105): p. 20 – 22.
48. Brust, M., et al., *Synthesis of thiol – derivatised gold nanoparticles in a two – phase Liquid – Liquid system.* Journal of the Chemical Society, Chemical Communications, 1994(7): p. 801 – 802.
49. Quintanilla, A., et al., *Weakly bound capping agents on gold nanoparticles in catalysis: Surface poison?* Journal of Catalysis, 2010. **271**(1): p. 104 – 114.
50. Kong, B. – S., J. Geng, and H. – T. Jung, *Layer – by – layer assembly of Graphene and gold nanoparticles by vacuum filtration and spontaneous reduction of gold ions.* Chemical Communications, 2009(16): p. 2174 – 2176.
51. Moussa, S., et al., *Laser assisted photocatalytic reduction of metal ions by Graphene oxide.* Journal of Materials Chemistry, 2011. **21**(26): p. 9608 – 9619.
52. Kamat, P.V., *Graphene – Based Nanoarchitectures. Anchoring Semiconductor and Metal Nanoparticles on a Two – Dimensional Carbon Support.* The Journal of Physical Chemistry Letters, 2009. **1**(2): p. 520 – 527.
53. Zhang, Y., et al., *Gold – silver nanocomposite – functionalized Graphene sensing platform for an electrochemiluminescent immunoassay of a tumor marker.* RSC Advances, 2013. **3**(34): p. 14701 – 14709.
54. Treguer – Delapierre, M., et al., *Synthesis of non – spherical gold nanoparticles.* Gold Bulletin, 2008. **41**(2): p. 195 – 207.
55. Yang, H., et al., *Uniform Decoration of Reduced Graphene Oxide Sheets with Gold Nanoparticles.* Journal of Nanotechnology, 2012. **2012**: p. 8.
56. Ki Kang, K., et al., *Enhancing the conductivity of transparent Graphene films via doping.* Nanotechnology, 2010. **21**(28): p. 285205.
57. Dai, B., et al., *High – quality single – layer Graphene via reparative reduction of Graphene oxide.* Nano Research, 2011. **4**(5): p. 434 – 439.
58. Zhang, Y. – L., et al., *Photoreduction of Graphene Oxides: Methods, Properties, and Applications.* Advanced Optical Materials, 2014. **2**(1): p. 10 – 28.
59. Fatt Teoh, H., et al., *Direct laser – enabled Graphene oxide–Reduced Graphene oxide layered structures with micropatterning.* Journal of Applied Physics, 2012. **112**(6): p. – .
60. Kundu, S., et al., *Effect of angstrom – scale surface roughness on the self – assembly of polystyrene – polydimethylsiloxane block copolymer.* Sci. Rep., 2012. **2**.
61. Krishnan, D., et al., *Energetic Graphene oxide: Challenges and opportunities.* Nano Today, 2012. **7**(2): p. 137 – 152.
62. Chen, W. and L. Yan, *Preparation of Graphene by a low – temperature thermal reduction at atmosphere pressure.* Nanoscale, 2010. **2**(4): p. 559 – 563.

63. Talapin, D.V., et al., *Evolution of an Ensemble of Nanoparticles in a Colloidal Solution: Theoretical Study.* The Journal of Physical Chemistry B, 2001. **105**(49): p. 12278 – 12285.
64. Kneipp, K., et al., *Surface – Enhanced Raman Spectroscopy in Single Living Cells Using Gold Nanoparticles.* Applied Spectroscopy, 2002. **56**(2): p. 150 – 154.
65. Kneipp, K., et al., *Detection and identification of a single DNA base molecule using surface – enhanced Raman scattering (SERS).* Physical Review E, 1998. **57**(6): p. R6281 – R6284.
66. Orendorff, C.J., et al., *Surface – Enhanced Raman Spectroscopy of Self – Assembled Monolayers: Sandwich Architecture and Nanoparticle Shape Dependence.* Analytical Chemistry, 2005. **77**(10): p. 3261 – 3266.
67. Vo – Dinh, T., et al., *Surface – enhanced Raman spectrometry for trace organic analysis.* Analytical Chemistry, 1984. **56**(9): p. 1667 – 1670.
68. Fleischmann, M., P.J. Hendra, and A.J. McQuillan, *Raman spectra of pyridine adsorbed at a silver electrode.* Chemical Physics Letters, 1974. **26**(2): p. 163 – 166.
69. Jasuja, K. and V. Berry, *Implantation and Growth of Dendritic Gold Nanostructures on Graphene Derivatives: Electrical Property Tailoring and Raman Enhancement.* ACS Nano, 2009. **3**(8): p. 2358 – 2366.
70. Goncalves, G., et al., *Surface Modification of Graphene Nanosheets with Gold Nanoparticles: The Role of Oxygen Moieties at Graphene Surface on Gold Nucleation and Growth.* Chemistry of Materials, 2009. **21**(20): p. 4796 – 4802.
71. Zihua, Z., Z. Tao, and L. Zhongfan, *Raman scattering enhancement contributed from individual gold nanoparticles and interparticle coupling.* Nanotechnology, 2004. **15**(3): p. 357.
72. Lu, G., et al., *Surface enhanced Raman scattering of Ag or Au nanoparticle – decorated reduced Graphene oxide for detection of aromatic molecules.* Chemical Science, 2011. **2**(9): p. 1817 – 1821.